

Synthesis of Diethyl Carbonate in Liquid Phase Oxidative Carbonylation over Activated Carbon-Supported Chloride-Free Cu-Based Catalysts

Hongbing Wang, Yao Xiang, Mingming Guo, Jiana Su, Gongying Wang, Wei Cui,* and Zhiyong Deng*



Cite This: *Energy Fuels* 2020, 34, 8697–8706



Read Online

ACCESS |

Metrics & More

Article Recommendations

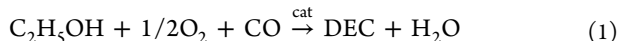
Supporting Information

ABSTRACT: Synthesis of diethyl carbonate (DEC) in the liquid phase by oxidative carbonylation of ethanol over activated carbon (AC) supported chloride-free Cu-based catalysts offers a prospective “green chemistry” strategy compared to the traditional preparation processes. The catalysts of Cu/AC were synthesized via a one-pot carbothermal method, and the Cu(+1) and Cu(0) valence distribution of Cu/AC catalyst was adjusted by simple carbon heat treatment. The physicochemical properties of the catalysts of Cu/AC were characterized by X-ray photoelectron spectroscopy, X-ray diffraction, transmission electron microscopy, and the Brunauer–Emmett–Teller model. The 10%-Cu/AC-873 catalyst (calcined at 873 K) exhibits the best catalytic activity for the synthesis of DEC under optimized conditions: $T = 393\text{ K}$, $P = 4.0\text{ MPa}$, $P_{\text{CO}}/P_{\text{O}_2} = 9:1$, and reaction time 2 h. The conversion of ethanol and space-time yield of DEC were 7.3% and $594.4\text{ mg}\cdot\text{g}^{-1}\cdot\text{h}^{-1}$, respectively. The 10%-Cu/AC-873 catalyst was reused four times without an obvious decrease in the activity. The adsorption energies of reactive species (CO , CH_3CHO , $\text{CH}_3\text{CH}_2\text{OCO}$) on Cu and Cu_2O were calculated by density functional theory; the results indicate that the synergic function of Cu^+ and Cu^0 enhanced the catalytic performance of Cu-based catalyst.

1. INTRODUCTION

Diethyl carbonate (DEC), as an important green chemical that has negligible ecotoxicity and high biodegradability, has been widely used as a fuel additive, lithium battery electrolyte, surfactant, solvent, etc.^{1–5} DEC has a better fuel/water distribution coefficient than dimethyl carbonate (DMC) and a higher oxygen content (40.6%) than methyl *tert*-butyl ether (MTBE) (18.2%)^{6,7} when used as an oxygen-containing fuel additive for gasoline and diesel fuels.⁸

The main synthetic methods of DEC include urea alcoholysis,^{7,9–11} transesterification of carbonate,^{12–15} direct synthesis route from ethanol and carbon dioxide (CO_2),^{16–18} and ethanol oxidative carbonylation.¹⁹ Many authors have reviewed these synthetic methods exhaustively.^{20–22} Notably, urea alcoholysis has a lower conversion rate because of evaporation of ethanol in the removal of ammonia during the reaction, transesterification of ethanol has a smaller equilibrium constant, carbonylation of ethanol using CO_2 is thermodynamically limited, and oxidative carbonylation of ethanol is a promising and quite favorable method because of its high atomic utilization rate. Its reaction formula is shown in eq 1.



CuCl is the traditional catalyst for the synthesis of DEC by ethanol oxidative carbonylation. However, due to the presence of chloride ions, the catalyst is highly corrosive to the alloy reactor. In order to overcome these problems, a number of catalysts have been explored to synthesize DEC. Li et al.²³ studied copper complex catalysts; 1,10-phenanthroline was found to effectively inhibit the corrosion by the catalyst of the

stainless steel reactor. Wang et al.²⁴ researched the role of ionic liquid in oxidative carbonylation of ethanol to synthesize DEC. It was found that not only may the ionic liquid facilitate the conversion of ethanol, but also it may effectively reduce the corrosion. Zhang et al.²⁵ investigated $\text{CuCl}-\text{PdCl}_2/\text{C}$ catalysts to catalyze ethanol to DEC using a continuous flow microreactor. Briggs et al.²⁶ investigated the role of KCl and NaOH on carbon-supported $\text{CuCl}_2/\text{PdCl}_2$ catalysts. Zhang et al.²⁷ employed a new type of catalyst, $\text{PdCl}_2/\text{Cu-HMS}$, for the synthesis of DEC. However, all of these studies are based on the development of chloride-containing catalysts, and chloride is easily eluted to form HCl, resulting in the catalytic activity decreasing subsequently and the equipment corroding seriously. Therefore, the development of chloride-free catalysts is becoming the main research direction. Shen et al.²⁸ investigated the oxidative carbonylation of ethanol occurring on $\text{Cu(I)}/\beta$ or $\text{Pd(II)}/\beta$ by density functional theory (DFT) calculations, proposing that DEC can form via two distinct reaction pathways. Both reaction pathways for the formation of DEC are accessible on $\text{Cu(I)}/\beta$ catalyst. Ren et al.²⁹ explored DMC formation on Rh-doped Cu/activated carbon (AC) surfaces by DFT study. Huang et al.³⁰ investigated the CuY catalyst for diethyl carbonate by oxycarbonylation in the vapor

Received: February 15, 2020

Revised: April 27, 2020

Published: May 1, 2020



phase. The research indicated that the acidity and type of Cu⁺ species were all responsible for the activity and product distribution. However, there are no reports about the synthesis of diethyl carbonate in liquid phase oxidative carbonylation over chloride-free Cu-based catalysts.

Based on the research above, we have fabricated chloride-free Cu-based catalysts *in situ* synthesized by carbothermal reduction. The preparation process of Cu/AC catalyst via a one-pot carbothermal method is simpler, more economical, and more environmentally friendly than the CuY catalyst, which was the only reported chlorine-free catalyst for the synthesis of DEC by oxidative carbonylation of ethanol. In addition, the valence distribution of Cu⁰ and Cu⁺ can be regulated by controlling the calcination time. This is of great significance for the controllable preparation of catalysts. In the present work, we investigated the effects of the preparation conditions of Cu/AC catalysts on the physicochemical properties and catalytic performance in the synthesis of DEC. Transmission electron microscopy (TEM), N₂ adsorption–desorption, X-ray photoelectron spectroscopy (XPS), and X-ray diffraction (XRD), were used to characterize the Cu/AC catalysts for the understanding of their structure–performance relationships. In addition, the adsorption energies of reactive species (CO, CH₃CHO, CH₃CH₂OCO) on Cu and Cu₂O were studied by DFT to comprehend the cooperation between Cu⁰ and Cu⁺ catalyzing the synthesis of diethyl carbonate from ethanol.

2. EXPERIMENTAL SECTION

2.1. Materials and Instruments. All chemical reagents were of AR grade and were used as received without further purification. Anhydrous ethanol, diethyl carbonate, acetaldehyde (ACE), and 1,1-diethoxyethane (DEE) were purchased from Shanghai Aladdin Bio-Chem Technology Co., Ltd. Cupric nitrate (Cu(NO₃)₂·3H₂O) was purchased from Sinopharm Chemical Reagent Co. Activated carbon (AC) was purchased from Shanghai Macklin Biochemical Co., Ltd. O₂ (>99.99%) and CO (>99.99%) were supplied by the Chengdu JinKeXing Gaseous Co., Ltd. A GS-0.1 autoclave was purchased from Weihai Chemical Machinery Co., Ltd.

2.2. Catalyst Preparation. The AC made from coconut shells (Shanghai Macklin Biochemical Co., Ltd. 20–50 mesh) was ground to 200–300 mesh. Prior to impregnation, the AC (200–300 mesh) was refluxed with HNO₃ (6 mol/L) at 373 K for 10 h, followed by washing with deionized water until pH 7 and eventually dried at 373 K for 10 h. Cu/AC catalysts were prepared by excessive wetness impregnation. A 2.0 g sample of AC was impregnated with an aqueous solution of Cu(NO₃)₂ and stirred for 6 h at room temperature. Subsequent to removal of the solvent by reduced pressure distillation, the obtained sample was dried at 373 K. The final catalysts were calcined at different temperatures under a nitrogen atmosphere for 4 h. The obtained catalysts were denoted as Cu/AC-*T*, where *T* represents the calcination temperature.

2.3. Characterization of Catalysts. The crystal structure of catalysts was identified by XRD (X'Pert PRO MPD) using a Cu K α radiation source (1.54056 Å). The patterns were recorded at a scanning rate at 5°/min in the range 10–85° under atmospheric pressure. The crystalline size was determined by Scherrer's equation: $D = K\lambda/\beta \cos \theta$, where $K = 0.9$. D and λ represent the crystallite size and the wavelength of Cu K α radiation, respectively. β is the corrected half-width of the diffraction peak.

The N₂ adsorption–desorption isotherms were measured with a Kubo-X1000 automatic physical adsorption analyzer (Beijing Builder Electronic Technology Co., Ltd.). The samples were degassed at 473 K for 3 h before analysis. The surface areas were determined with the use of the Brunauer–Emmett–Teller (BET) model, and the pore size

distributions were calculated by the BJH (Barrett–Joyner–Halenda) method from the desorption branch.

The morphologies of the catalysts were characterized by transmission electron microscopic (TEM) photographs with an FEI TECNAI G2 F20. The average particle size was calculated with nano measurer software from TEM image analysis.

X-ray photoelectron spectroscopy (XPS) was recorded on a Thermo ESCALAB 250XI X-ray photoelectron spectrometer (Thermo, USA) using Al K $\alpha_{1,2}$ monochromatized radiation at a 16 kV X-ray source. Quantitative determination of the Cu was performed by ICP-OES.

2.4. Catalyst Performance. All the experiments were conducted with a 100 mL stainless steel autoclave; 0.8 g of catalyst and 20 mL of ethanol were added into the reactor. After the air was replaced in the autoclave three times, it was then pressurized to 3.6 MPa with CO and 0.4 MPa with O₂, respectively. After the temperature rose to 393 K and reaction occurred for 2 h, the reactor was placed into an ice–water bath and cooled to room temperature. The products were analyzed with an Agilent 7820A gas chromatograph equipped with a thermal conductivity detector (TCD). The byproducts observed included 1,1-diethoxyethane (DEE) and acetaldehyde (ACE). The conversion of ethanol (C_{EtOH}), DEC selectivity (S_{DEC}), and the space-time yield of DEC (STY_{DEC}) were determined by eqs 2–5:

$$C_{EtOH} = \frac{\frac{2x_{DEC}}{M_{DEC}} + \frac{3x_{DEE}}{M_{DEE}} + \frac{x_{ACE}}{M_{ACE}}}{\frac{x_{Et}}{M_{Et}} + \frac{2x_{DEC}}{M_{DEC}} + \frac{3x_{DEE}}{M_{DEE}} + \frac{x_{ACE}}{M_{ACE}}} \quad (2)$$

$$S_{DEC} = \frac{\frac{2x_{DEC}}{M_{DEC}}}{\frac{2x_{DEC}}{M_{DEC}} + \frac{3x_{DEE}}{M_{DEE}} + \frac{x_{ACE}}{M_{ACE}}} \quad (3)$$

$$S_{DEE} = \frac{\frac{3x_{DEE}}{M_{DEE}}}{\frac{2x_{DEC}}{M_{DEC}} + \frac{3x_{DEE}}{M_{DEE}} + \frac{x_{ACE}}{M_{ACE}}} \quad (4)$$

$$\begin{aligned} STY_{DEC} &= \frac{m_{DEC}}{m_{cat} t} \\ &= \frac{V_{Et} \rho_{Et} C_{EtOH} S_{DEC} M_{DEC}}{2M_{Et}} \frac{1}{m_{cat} t} \end{aligned} \quad (5)$$

x_{DEC} , x_{ACE} , x_{DEE} , and x_{Et} are the mass fractions of the liquid components of DEC, ACE, DEE, and EtOH. V_{Et} is the volume of EtOH; M_{DEC} , M_{ACE} , M_{DEE} , and M_{Et} are the relative molecular masses of DEC, ACE, DEE, and EtOH; ρ_{Et} is the density of EtOH (0.789 g/mL); m_{cat} is the quality of catalyst.

3. RESULTS AND DISCUSSION

3.1. Characterization of Catalyst. **3.1.1. X-ray Diffraction.** The XRD patterns of AC, Cu/AC-673, Cu/AC-773, Cu/AC-873, Cu/AC-973, and Cu/AC-1073 are given in Figure 1. The characteristic diffraction peak of the sample near $2\theta = 26.3^\circ$ is attributed to the (002) crystal plane of graphitic carbon. The peaks at 43, 50, and 73.9° correspond to (111), (200), and (220) of Cu (JCPDS 02-1225), respectively, while the peaks at 36.4, 42.2, and 61.3° are related to (111), (200), and (220) of Cu₂O (JCPDS 03-0892). These results are basically consistent with the literature report.^{31,32} The presence of Cu and Cu⁺ species suggests that the copper precursors were reduced by the carbothermal method.^{33,34} As illustrated in Figure 1, there is hardly any characteristic diffraction peak of Cu(111) in the Cu/AC-673 sample. With the increase of calcination temperature, the characteristic diffraction peaks of Cu gradually increased while the Cu₂O progressively reduced. XRD patterns of samples show that the phase composition was dependent on the calcination temperature. This is mainly due

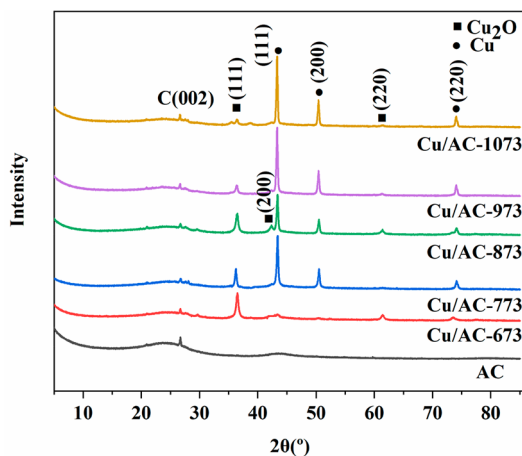


Figure 1. XRD patterns of Cu/AC at different calcination temperatures.

to the reduction of $\text{Cu}(\text{NO}_3)_2$ by AC with the order $\text{Cu}^{2+} \rightarrow \text{Cu}^+ \rightarrow \text{Cu}$ during the progress of calcination.^{35,36} Meanwhile, the formation of CO and CO_2 causes cavities on the AC, which increases the specific surface areas of Cu/AC catalysts. The S_{BET} values of Cu/AC catalysts increase from 692.6 to 948.4 m^2/g (at 673–1073 K).

Figure 2 shows the XRD patterns of different Cu loadings. The characteristic diffraction peaks of different crystal planes of

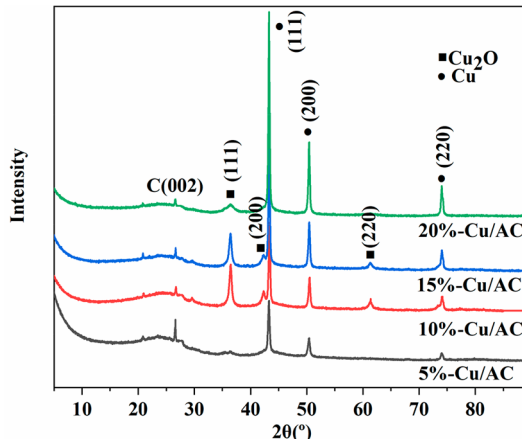


Figure 2. XRD patterns of Cu/AC at different loads.

Cu show higher and sharper intensities with the increase of Cu loading, which indicates the formation of more Cu species. However, the characteristic diffraction peak of the intensity of $\text{Cu}_2\text{O}(111)$ shows a tendency of first increasing and later decreasing. In addition, the size of Cu nanoparticles (NPs) is obviously affected by Cu loading; the size of Cu NPs increases from 28.7 to 37.3 nm with the increase of loading from 5 to 20% (calculated from the XRD based on the Scherrer equation; see Table 5).

3.1.2. X-ray Photoelectron Spectroscopy. XPS was investigated to analyze the valence states of Cu components on the surfaces of the catalyst. As shown in Figure 3, all Cu/AC catalysts had two peaks centered at ca. 932.7 and 952.5 eV, which are related to the $\text{Cu } 2\text{p}_{1/2}$ and $\text{Cu } 2\text{p}_{3/2}$ peaks, respectively.^{37,38} These indicate that Cu components are successfully reduced into zerovalent states by the carbothermal method. However, Cu^0 and Cu^+ cannot be distinguished

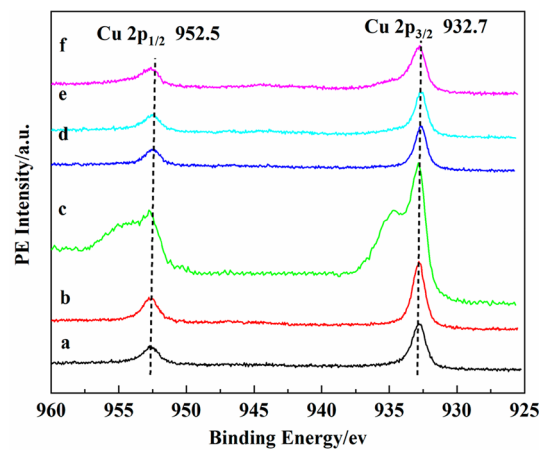


Figure 3. Cu 2p XPS spectra of different catalysts. (a) 10%-Cu/AC-673, (b) 10%-Cu/AC-773, (c) 10%-Cu/AC-873, (d) 10%-Cu/AC-973, (e) 10%-Cu/AC-1073, and (f) 10%-Cu/AC-873 after used four times.

because their binding energies are very close. Cu LMM XAS spectra (Figure 4) can distinguish them from their position in

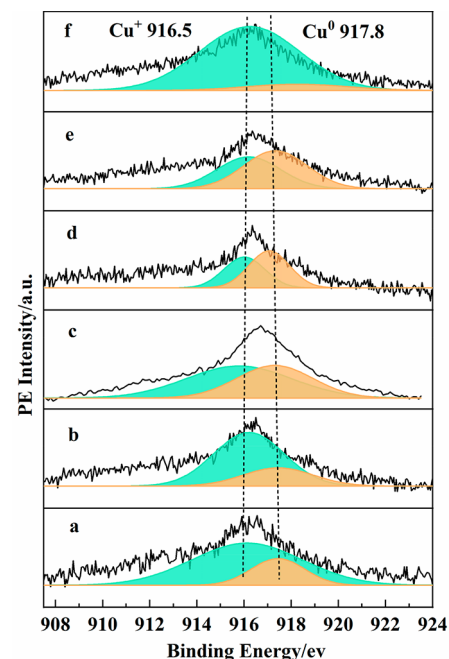


Figure 4. Cu LMM XAS spectra of different catalysts. (a) 10%-Cu/AC-673, (b) 10%-Cu/AC-773, (c) 10%-Cu/AC-873, (d) 10%-Cu/AC-973, (e) 10%-Cu/AC-1073, and (f) 10%-Cu/AC-873 after used four times.

XPS spectra; the peaks are observed at ca. 916.5 and 917.8 eV corresponding to Cu^+ and Cu^0 , respectively.³⁰ The values of Cu^0/Cu^+ of Cu components on the surfaces of catalysts from the Cu LMM XAS spectra were obtained. As listed in Table 1, the value of Cu^0/Cu^+ varied in the order Cu/AC-1073 > Cu/AC-973 > Cu/AC-873 > Cu/AC-773 > Cu/AC-673, which indicates that carbothermal method can adjust Cu(+1) and Cu(0) valence distribution of Cu/AC.

3.1.3. N_2 Adsorption–Desorption. The N_2 adsorption–desorption isotherms in Figure 5A show that the Cu/AC catalysts possess mesoporous structure belonging to typical IV adsorption curves with clear hysteresis loops under medium

Table 1. Surface Cu Compositions of Cu/AC Catalysts Based on Cu 2p_{3/2} XPS and Cu LMM Deconvolution

catalyst	BE of Cu 2p _{3/2} (eV)		KE of Cu LMM (eV)		area of Cu 2p _{3/2} (%)		area of Cu LMM (%)		Cu ⁰ /Cu ⁺
	Cu ²⁺	Cu ⁺ + Cu ⁰	Cu ⁺	Cu ⁰	Cu ²⁺	Cu ⁺ + Cu ⁰	Cu ⁺	Cu ⁰	
Cu/AC-673	934.0	932.6	916.6	917.9	74.0	26.0	88.1	11.9	0.14
Cu/AC-773	933.9	932.8	916.2	917.5	69.9	30.1	74.6	25.4	0.34
Cu/AC-873	934.5	932.9	916.5	917.8	64.0	36.0	52.0	48.0	0.92
Cu/AC-973	934.0	932.7	916.0	917.1	36.8	63.2	40.4	59.6	1.48
Cu/AC-1073	934.2	932.6	916.2	917.3	15.4	84.6	36.6	63.4	1.73
Cu/AC-4 ^a	933.7	932.0	916.3	918.0	78.0	22.0	91.1	8.9	0.10

^aCu/AC-4 after used four times.

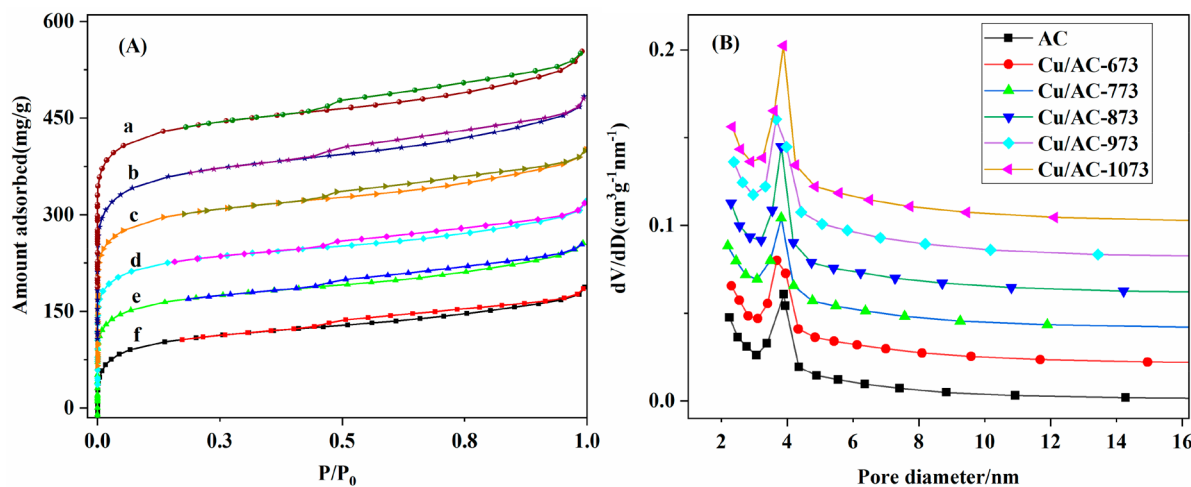


Figure 5. (A) N₂ adsorption–desorption isotherm of Cu/AC catalysts under different calcination temperatures: (a) AC, (b) 10%-Cu/AC-673, (c) 10%-Cu/AC-773, (d) 10%-Cu/AC-873, (e) 10%-Cu/AC-973, and (f) 10%-Cu/AC-1073. (B) Pore diameter based on BJH of Cu/AC catalysts under different calcination temperatures.

relative pressures of 0.4–0.8, which was consistent with capillary condensation in mesopores (2–5 nm), in accordance with the pore size distribution in Figure 5B. Table 2 lists the

Table 2. Surface Areas and Pore Structures of the Catalysts

catalyst	S _{BET} (m ² /g)	V _p (cm ³ /g)	D _p (nm)	D _p ^a (nm)
AC	966.2	0.62	3.90	
Cu/AC-673	692.6	0.43	3.69	41.50
Cu/AC-773	729.5	0.45	3.82	28.70
Cu/AC-873	894.7	0.53	3.82	14.28
Cu/AC-973	965.1	0.57	3.84	91.86
Cu/AC-1073	948.4	0.58	3.89	190
Cu/AC-4	715.8	0.33	3.69	13.12

^aCopper particle size determined by TEM. Cu/AC-4: after used four times.

detailed structural parameters of these samples. It shows that the S_{BET}, pore volume, and mean pore size of Cu/AC catalysts are significantly smaller than those in AC. These characteristics indicate that the Cu species entered the pores of AC.³⁹ TEM analyses of the catalysts have been carried out to further verify this hypothesis (Figure 6).

3.1.4. TEM. TEM images of Cu/AC catalysts under different calcination temperatures are used to observed the sizes of Cu NPs. As shown in Figure 6, Cu NP sizes were about 41.50 nm on Cu/AC-673, 28.70 nm on Cu/AC-773, 14.28 nm on Cu/AC-873, 91.86 nm on Cu/AC-973, 190 nm on Cu/AC-1073, and 13.12 nm on Cu/AC-4 (after it was used four times). The increase of Cu NP size with calcination temperature from 673

to 1073 K indicated the heat treatment temperature led to a serious agglomeration of Cu NPs on the surface of the support. Furthermore, the lattice fringes can be clearly distinguished with d-spacings of 0.208 and 0.246 nm from the high-resolution TEM (HRTEM) images in Figure 6. The characteristic diffraction peaks of the Cu(111) and Cu₂O(111) facets could be observed in the XRD patterns (Figure 1), and the values of the d-spacing from the TEM were also close to the values of the PDF cards (JCPDS 02-1225, JCPDS 03-0892). Consequently, the lattice fringes could be assigned to the Cu(111) and Cu₂O(111) facets. This is consistent with previously reported literature.^{31,40}

3.2. Catalytic Performance. **3.2.1. Effect of Synthesis Parameters of Catalyst on Activity.** First, the parameter of calcination time on oxidative carbonylation of EtOH was explored. Table 3 lists the catalytic performance of a series of 10%-Cu/AC catalysts in oxidative carbonylation of ethanol, which are calcined under 873 K. As listed in Table 3, ethanol conversion and space-time yield (STY) of DEC increase at first and then decrease with the rises of calcination time. The optimal calcination time is considered to be 4 h, with the highest conversion of EtOH and STY of DEC of 7.3% and 594.4 mg·g⁻¹·h⁻¹, respectively. Therefore, the calcination time for the subsequent catalyst preparation is 4 h. After that, we investigated the effect of calcination temperature on the oxidation carbonylation of EtOH. As listed in Table 4, ethanol conversion and STY of DEC increase at first and then decrease with the calcination temperature from 673 to 1073 K. Nevertheless, DEE selectivity always rises. The 10%-Cu/AC-873 catalyst performs the highest ethanol conversion and STY

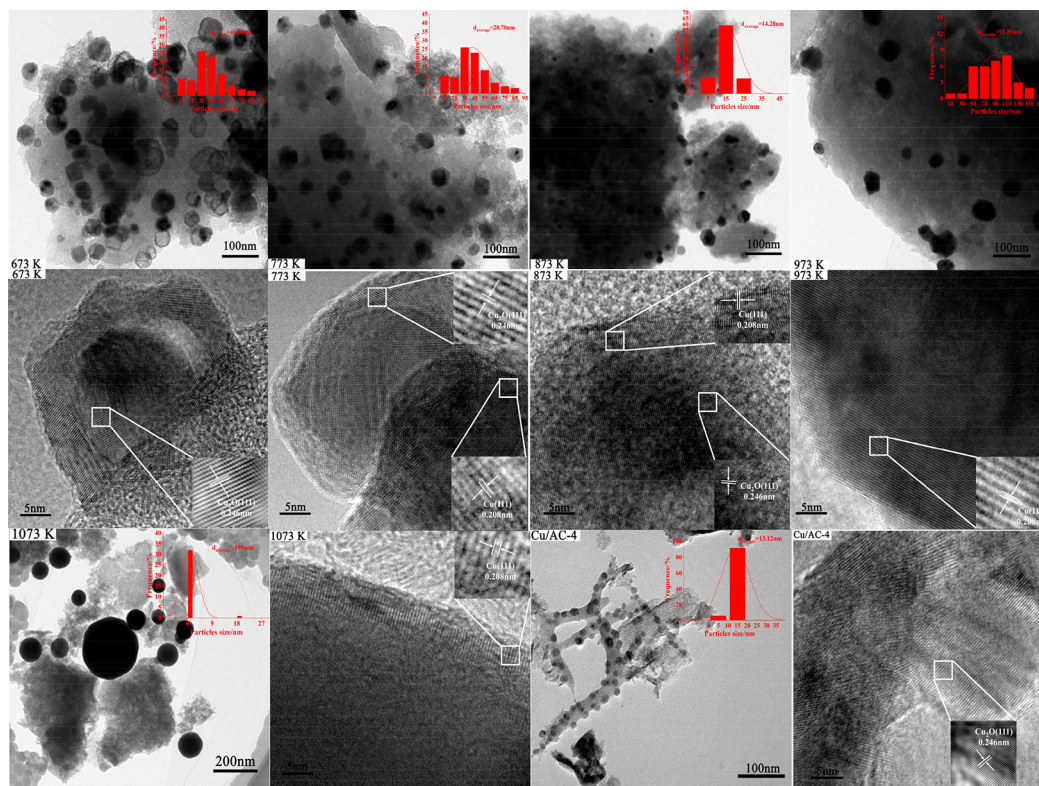


Figure 6. TEM images of 10%-Cu/AC catalysts (insets, Cu NP size distribution plots) and their corresponding HRTEM images. Cu/AC-4: after used four times.

Table 3. Catalytic Performances of Catalysts at Different Calcination Times^a

catalyst	calcination (h)	EtOH conv (%)	selectivity (%)			STY _{DEC} (mg·g ⁻¹ ·h ⁻¹)
			DEC	DEE	ACE	
10%-Cu/AC-873	1	3.9	52.5	21.2	25.7	259.3
10%-Cu/AC-873	2	4.4	53.7	22.2	23.8	299.2
10%-Cu/AC-873	3	4.8	52.8	25.9	21.0	320.9
10%-Cu/AC-873	4	7.3	64.3	31.2	3.8	594.4
10%-Cu/AC-873	5	5.1	52.4	28.8	17.9	338.4
10%-Cu/AC-Re	6	5.1	52.4	27.8	18.5	338.4
10%-Cu/AC-Ox	6	0	0	0	0	0

^aReaction conditions: 393 K; 2 h; 4.0 MPa; $P_{CO}/P_{O_2} = 9:1$; catalyst, 0.8 g; 20 mL of ethanol; stirring rate, 600 rpm. 10%-Cu/AC-Re, reduced in H₂ at 573 K for 6 h; 10%-Cu/AC-Ox, calcined in air at 473 K for 6 h.

Table 4. Catalytic Performances of Catalysts at Different Calcination Temperatures^a

catalyst	EtOH conv (%)	selectivity (%)			STY _{DEC} (mg·g ⁻¹ ·h ⁻¹)
		DEC	DEE	ACE	
AC	0	0	0	0	0
Cu/AC-673	4.5	58.2	25.8	14.9	328.8
Cu/AC-773	5.8	59.8	30.9	8.4	449.6
Cu/AC-873	7.3	64.3	31.2	3.8	594.4
Cu/AC-973	1.9	45.9	32.4	20.7	112.3
Cu/AC-1073	1.1	40.5	48.6	9.2	57.8

^aReaction conditions: 393 K; 2 h; 4.0 MPa; $P_{CO}/P_{O_2} = 9:1$; catalyst, 0.8 g; 20 mL of ethanol; stirring rate, 600 rpm.

of DEC (7.3%, 594.4 mg·g⁻¹·h⁻¹). The highest catalytic activity of the 10%-Cu/AC-873 catalyst should be attributed to the following two reasons.

First, the reducibility of Cu species by a one-pot carbothermal method is a crucial factor in its catalytic performance. Literature reports that the active component for the oxidative carbonylation of ethanol is Cu⁺.³⁰ In order to determine the active sites of Cu/AC catalyst in the oxidative carbonylation of EtOH to DEC, the 10%-Cu/AC-873 catalyst was calcined in an air atmosphere at 473 K and reduced in H₂ at 573 K for 6 h, respectively. The obtained sample (10%-Cu/AC-Ox) is mainly composed of CuO (Figure S1) and displays no activity in the oxidative carbonylation of EtOH to DEC (Table 3, Figure 3, and Figure 4) also indicate that the active sites are Cu⁰ and Cu⁺ rather than CuO.

Second, the 10%-Cu/AC-873 catalyst has a moderate ratio of Cu⁰ to Cu⁺. Table 1 and Figure 4 show that the value of Cu⁰/Cu⁺ increases with the rise of calcination temperature from 673 to 1073 K. It is notable that the surface content of Cu²⁺ and Cu⁺ decreased while Cu⁰ increased with the rise of calcination temperature. The relationship between catalytic

activity and the value of Cu^0/Cu^+ is shown in Figure 7. It can be seen that optimal catalytic activity for 10%-Cu/AC-873 is

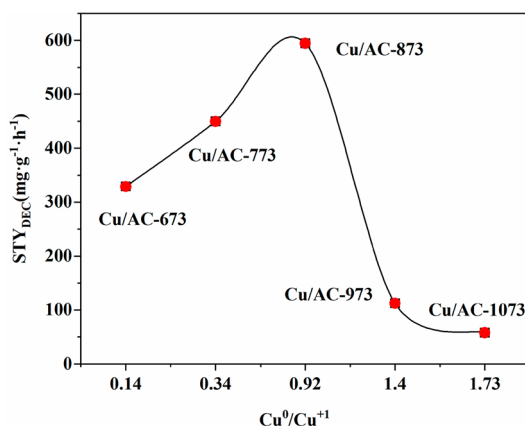


Figure 7. Relationship between catalytic activity and the ratio of Cu^0/Cu^+ .

obtained for a STY_{DEC} of $594.4 \text{ mg}\cdot\text{g}^{-1}\cdot\text{h}^{-1}$, which can be assigned to favorable valence distribution of Cu species ($\text{Cu}^0/\text{Cu}^+ = 0.92$). In addition, as shown in Figure 1, the characteristic diffraction peak intensity of $\text{Cu}(111)$ gradually increases while that of $\text{Cu}_2\text{O}(111)$ decreases with the calcination temperature increasing from 673 to 1073 K. The 10%-Cu/AC-873 catalyst exhibits a medium-intensity characteristic diffraction peak, which is well consistent with catalytic activities (Table 4).

The effect of Cu loading on the oxidative carbonylation of EtOH was also examined (Table 5). With the increase of Cu loading from 5 to 20%, the conversion of ethanol and STY of DEC increase at first and then decrease; the 10%-Cu/AC-873 catalyst performs optimum catalytic activity. It is distinguished that the conversion of ethanol and STY of DEC began to decline when the Cu load exceeded 10%. This contributes to the agglomeration of Cu NPs (Table 5 and Figure 2).

3.2.2. Optimization of Reaction Conditions. CO is the carbonyl source in the oxidative carbonylation of ethanol. Consider that the explosion limit of the mixture of CO and air is 12.5–74.2%.⁴¹ Therefore, the effect of the pressure ratio of CO to O_2 on the reaction performance was investigated. As shown in Figure 8a, when the total pressure is 4.0 MPa, the conversion of ethanol shows a trend of increasing first and then decreasing with the increase of the $P_{\text{CO}}/P_{\text{O}_2}$; the highest conversion is 7.3% ($P_{\text{CO}}/P_{\text{O}_2} = 9:1$). Although the selectivity of DEC slightly increases when the $P_{\text{CO}}/P_{\text{O}_2}$ improves, the conversion of ethanol drops significantly. The possible reason

is that fewer intermediate ethoxy groups are formed when the oxygen content is low. Hence, $P_{\text{CO}}/P_{\text{O}_2} = 9:1$ is to be selected as the optimal pressure ratio under the total pressure of 4.0 MPa.

The influence of reaction temperature on the oxidation carbonylation of ethanol over the 10%-Cu/AC-873 catalyst was investigated, and the result is shown in Figure 8b. The conversion of ethanol and the DEC selectivity were 5.6% and 50.4%, respectively, under the reaction temperature of 383 K. As the temperature rose, the conversion of ethanol gradually increased. When the temperature was 383 K, the ethanol conversion rate reached 7.3%, and the DEC selectivity was 64.3%. However, the conversion of ethanol was basically unchanged, but the selectivity of DEC began to decrease when the reaction temperature was further increased. This may contribute to increasing reaction temperature to some extent: ethanol is more oxidized to acetaldehyde leading to producing DEE by aldol condensation reaction.⁴² Therefore, the optimal reaction temperature is selected to be 383 K.

The effect of reaction time is shown in Figure 8c. When the reaction time is 2 h, the ethanol conversion rate is 7.3% and the DEC selectivity is 64.3%. However, the conversion of ethanol did not change significantly by raising the reaction time, but the DEC selectivity decreased slowly. The reason is that the side reaction was exacerbated as the reaction time increased. Therefore, 2 h was selected as the optimal reaction time.

3.2.3. Recyclability of Catalyst. The recyclability of the Cu/AC-873 catalyst had been investigated in the oxidative carbonylation of ethanol. As shown in Figure 9, the Cu/AC-873 catalyst was used four times with little decrease of EtOH conversion and DEC selectivity. In order to research the reason for the decrease in activity, the content of copper before and after four times of use was detected by ICP-OES. The results show that the copper content in the catalyst after four times of use is reduced to 7.66%, which is 2.3% lower than in fresh catalysts (9.96%). On the other hand, the loss of catalytic activity is related to the ratio of Cu^0/Cu^+ in Cu/AC-873. It was notable that $\text{Cu}^0/\text{Cu}^+ = 0.10$ after four times of reuse (Figure 4f), which is less than the value of 0.92 for the fresh catalyst. This is consistent with XRD patterns of Cu/AC after four times of use (Figure S2). As shown in Figure S2, the characteristic diffraction peaks of $\text{Cu}(111)$ gradually decreased while those of $\text{Cu}_2\text{O}(111)$ progressively increased. This shows that the Cu NPs are partially oxidized to Cu_2O after the catalyst is used four times, resulting in an imbalance of the Cu^0/Cu^+ ratio. In addition, the BET, pore volume, and mean pore size of Cu/AC-4 are slightly smaller than those of fresh

Table 5. Catalytic Performances of Different Loadings for Cu/AC-873 Catalysts^a

catalyst	EtOH conv (%)	selectivity (%)			$\text{STY}_{\text{DEC}} (\text{mg}\cdot\text{g}^{-1}\cdot\text{h}^{-1})$	$D^b (\text{nm})$
		DEC	DEE	ACE		
0%-Cu/AC-873	0	0	0	0	0	0
5%-Cu/AC-873	3.5	55.2	29.8	14.4	224.7	28.7
10%-Cu/AC-873	7.3	64.3	31.2	3.8	594.4	31.8
15%-Cu/AC-873	4.5	58.4	33.9	6.8	332.8	33.4
20%-Cu/AC-873	4.0	52.7	36.9	9.4	267.0	37.3

^aReaction conditions: 393 K; 2 h; 4.0 MPa; $P_{\text{CO}}/P_{\text{O}_2} = 9:1$; catalyst, 0.8 g; 20 mL of ethanol; stirring rate, 600 rpm. ^bCrystal size calculated at $2\theta = 36.4^\circ$ for $\text{Cu}(111)$ from XRD diffraction peaks based on the Scherrer equation.

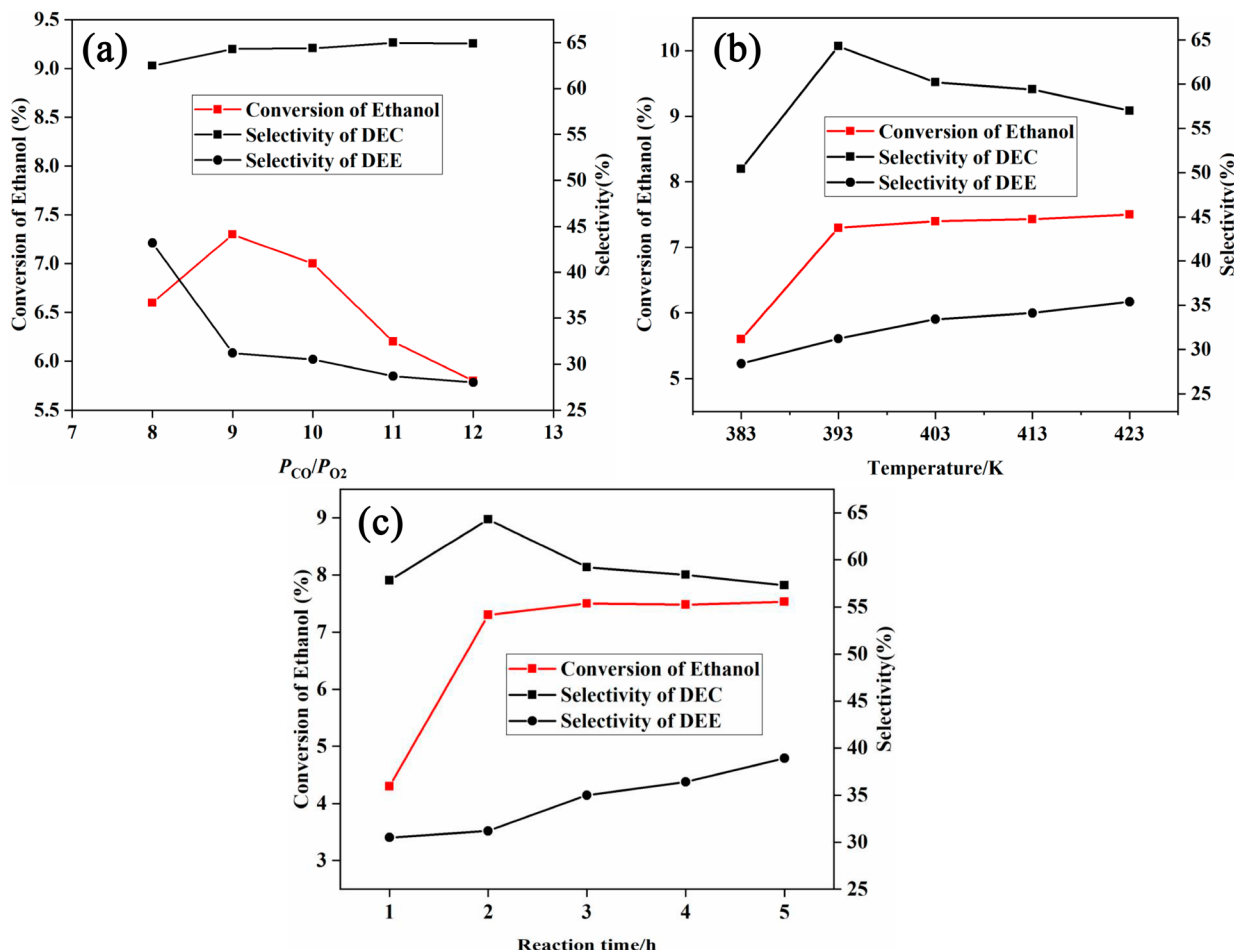


Figure 8. Conversion and selectivity in different reaction parameters: (a) reaction pressure ratio of CO/O₂ (2 h, 4.0 MPa, 393 K, 600 rpm, 20 mL of ethanol, 0.8 g of catalyst); (b) reaction temperature (2 h, 4.0 MPa, $P_{CO}/P_{O_2} = 9:1$, 600 rpm, 20 mL of ethanol, 0.8 g of catalyst). (c) reaction time (393 K, 4.0 MPa, $P_{CO}/P_{O_2} = 9:1$, 600 rpm, 20 mL of ethanol, 0.8 g of catalyst).

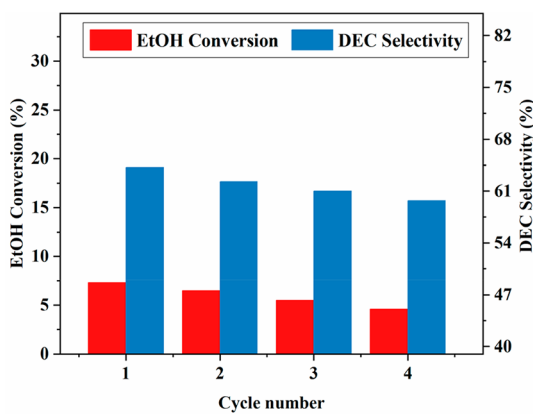
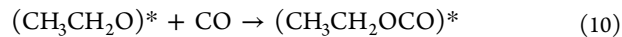
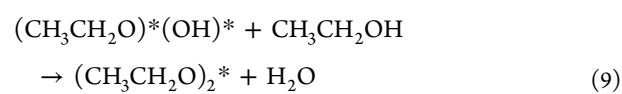


Figure 9. Catalyst recyclability. Reaction conditions: 393 K, 4.0 MPa ($P_{CO}/P_{O_2} = 9:1$), 600 rpm, 20 mL of ethanol, 0.8 g of catalyst.

catalyst (Table 2). However, the size of Cu NPs measured by TEM (Figure 6) did not increase.

3.2.4. Computational Results. Investigations of the active sites in Cu zeolites for the oxidative carbonylation of ethanol have been reported in the literature. Huang et al. found that the catalytic performances were in line with the proportions of Cu⁺ in CuY catalyst.³⁰ In order to understand the relationship between the catalytic activities and active sites (Cu⁰ and Cu⁺),

a DFT simulation has been carried out in this section (Figure 10) (see the detailed calculation method in the Supporting Information). Many works of literature have reported the mechanisms of DEC formation via experimental and theoretical calculation methods.^{28,43–50} The proposed reaction mechanism of DEC formation is illustrated by reactions 6–12.



In the mechanism given by reactions 6–12, the active site is denoted with an asterisk. (M)^{*} is used to represent an active site interacting with species M. This indicates that the insertion of CO into the CH₃CH₂O species to produce the CH₃CH₂OCO intermediate (reaction 10) is considered to

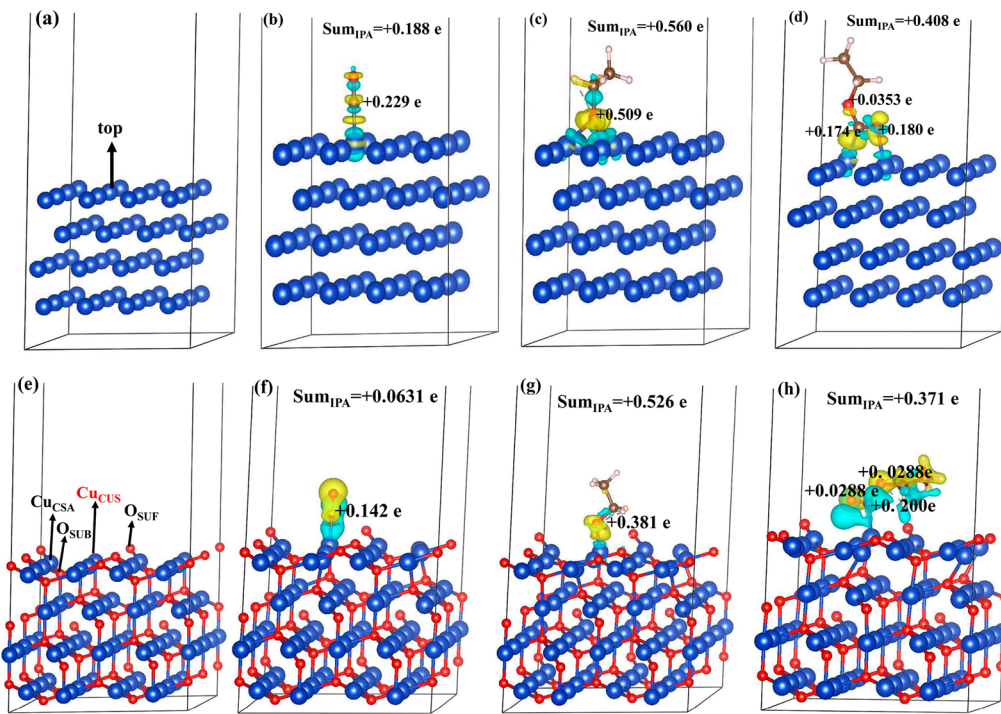


Figure 10. Three-dimensional charge density difference plot for Cu(111) (b–d) and Cu₂O(111) (f–h) adsorbed CO, CH₃CH₂O, and CH₃CH₂OCO, respectively. Yellow and light blue represent charge accumulation and depletion, respectively.

be the rate-determining step.⁵⁰ Based on the previous research that the preferred sites of intermediates and reactants prefer to adsorb on the top site of the Cu(111) surface and the coordinatively unsaturated site of Cu₂O(111) (Cu_{cus})^{45,46} we calculated the adsorption energies (E_{ads}) of CO, CH₃CH₂O, and CH₃CH₂OCO on Cu(111) and Cu₂O(111), respectively. As listed in Table 6, the adsorption distances of Cu–C(O) on

CH₃CH₂O species to produce the CH₃CH₂OCO intermediate. This result is consistent with the experimental results. As shown in Tables 1 and 4, when the Cu⁰/Cu⁺ value is the largest (Cu⁰/Cu⁺ = 1.73), DEE has the highest selectivity (48.6%). However, the conversion of ethanol is lower when the Cu⁰/Cu⁺ value is smaller. The catalyst of 10%-Cu/AC-873 has a high catalytic activity attributed to balancing the distribution of Cu species (Cu⁰/Cu⁺ = 0.92).

Table 6. Adsorption Energies for CO, CH₃CH₂O, and CH₃CH₂OCO Adsorbed at the Top Site of Cu(111) Surface (Cu_{cus}) of Cu₂O(111) Surface

surface	adsorption molecules	$d_{(\text{C}-\text{O})}$ (Å)	$d_{(\text{Cu}-\text{C}(\text{O}))}$ (Å)	E_{ads} (eV)
Cu(111)	CO	1.161 (1.162 ⁵¹)	1.860 (1.870 ⁵¹)	-0.410 (-0.420 ⁵¹)
	CH ₃ CH ₂ O	1.452	2.070	-2.080
	CH ₃ CH ₂ OCO	1.372, 1.220	1.960	-0.730
Cu ₂ O(111)	CO	1.140 (1.146 ⁵²)	1.790 (1.790 ⁵²)	-1.750 (1.610 ⁵²)
	CH ₃ CH ₂ O	1.410	1.780	-2.910
	CH ₃ CH ₂ OCO	1.230, 1.340	1.900	-2.290

Cu₂O(111) and Cu(111) are 1.790 and 1.860 Å, respectively, which is a significant increase relative to free CO molecules. This indicates that the CO adsorption causes the weakening of the C–O bond of CO, which is conducive to the further activation of CO. In addition, the E_{ads} of CH₃CH₂OCO on Cu₂O(111) surface is much lower than the E_{ads} on Cu(111), indicating the intermediates and reactants are more easily absorbed on Cu₂O(111). The high catalytic activity for the oxidation carbonylation of ethanol to DEC results from a cooperative effect between Cu⁰ and Cu⁺. Cu⁰ sites could accelerate the oxidation of ethanol to form CH₃CH₂O species, while Cu⁺ sites facilitate the insertion of CO into the

4. CONCLUSION

Cu/AC catalyst has been prepared using the one-pot carbothermal method. The 10%-Cu/AC-873 catalyst obtained at 873 K exhibits good performance for the synthesis of DEC by oxidation carbonylation of ethanol with 7.3% conversion of ethanol and 594.4 mg·g⁻¹·h⁻¹ STY of DEC within 2 h under a reaction temperature of 393 K and 4.0 MPa pressure ($P_{\text{CO}}/P_{\text{O}_2}$ = 9:1), which could be ascribed to the appropriate ratio of Cu⁰/Cu⁺. Moreover, the catalyst could be repeatedly used four times without any obvious decrease in catalytic activity. The main reasons for the catalyst deactivation after the fourth use are the loss of copper and the imbalance of the Cu⁰/Cu⁺ ratio caused by partial copper oxidation. DFT calculations provide a further understanding of the catalytic activities of catalysts. The high catalytic activity for oxidative carbonylation of EtOH to DEC results from a cooperative effect between Cu⁺ and Cu⁰.

ASSOCIATED CONTENT

Supporting Information

The Supporting Information is available free of charge at <https://pubs.acs.org/doi/10.1021/acs.energyfuels.0c00528>.

XRD patterns of 10%-Cu/AC-Re, 10%-Cu/AC-Ox, and Cu/AC catalysts; computational details (PDF)

AUTHOR INFORMATION

Corresponding Authors

Wei Cui – School of Chemical Sciences, University of Chinese Academy of Sciences, Beijing 100049, China; Email: cuiwei@ucas.ac.cn

Zhiyong Deng – Chengdu Institute of Organic Chemistry, Chinese Academy of Sciences, Chengdu 610041, Sichuan, China; National Engineering Laboratory for VOCs Pollution Control Material & Technology, University of Chinese Academy of Sciences, Beijing 101408, China; Email: zhiyongdeng@cioc.ac.cn

Authors

Hongbing Wang – Chengdu Institute of Organic Chemistry, Chinese Academy of Sciences, Chengdu 610041, Sichuan, China; National Engineering Laboratory for VOCs Pollution Control Material & Technology, University of Chinese Academy of Sciences, Beijing 101408, China; orcid.org/0000-0002-1952-415X

Yao Xiang – School of Chemical Sciences, University of Chinese Academy of Sciences, Beijing 100049, China

Mingming Guo – School of Chemical Sciences, University of Chinese Academy of Sciences, Beijing 100049, China

Jiana Su – Chengdu Institute of Organic Chemistry, Chinese Academy of Sciences, Chengdu 610041, Sichuan, China; National Engineering Laboratory for VOCs Pollution Control Material & Technology, University of Chinese Academy of Sciences, Beijing 101408, China

Gongying Wang – Chengdu Institute of Organic Chemistry, Chinese Academy of Sciences, Chengdu 610041, Sichuan, China; National Engineering Laboratory for VOCs Pollution Control Material & Technology, University of Chinese Academy of Sciences, Beijing 101408, China

Complete contact information is available at:

<https://pubs.acs.org/10.1021/acs.energyfuels.0c00528>

Notes

The authors declare no competing financial interest.

ACKNOWLEDGMENTS

We are thankful for the financial support provided by the Project Supported by Sichuan Province Science Foundation for Outstanding Youth Fund Training Program (2016JQ0062). The authors also would like to thank Ting Du from Shiyanjia Lab (www.shiyanjia.com) for the XPS, TEM, and XRD tests.

REFERENCES

- (1) Dong, J. J.; Roger, J.; Verrier, C.; Martin, T.; Le Goff, R.; Hoarau, C.; Doucet, H. Carbonates: eco-friendly solvents for Palladium-Catalysed Direct Arylation of Heteroaromatics. *Green Chem.* **2010**, *12* (11), 2053–2063.
- (2) Moumouzias, G.; Ritzoulis, G.; Siapkas, D.; Terzidis, D. Comparative study of LiBF₄, LiAsF₆, LiPF₆, and LiClO₄ as electrolytes in propylene carbonate–diethyl carbonate solutions for Li/LiMn₂O₄ cells. *J. Power Sources* **2003**, *122* (1), 57–66.
- (3) Sakakura, T.; Kohno, K. The Synthesis of Organic Carbonates from Carbon Dioxide. *Chem. Commun.* **2009**, No. 11, 1312–1330.
- (4) Tobiszewski, M.; Zabrocka, W.; Bystrzanowska, M. Diethyl Carbonate as a Green Extraction solvent for Chlorophenol Determination with Dispersive Liquid–Liquid Microextraction. *Anal. Methods* **2019**, *11* (6), 844–850.
- (5) Yan, C.; Yao, Y.-X.; Chen, X.; Cheng, X.-B.; Zhang, X.-Q.; Huang, J.-Q.; Zhang, Q. Lithium Nitrate Solvation Chemistry in

Carbonate Electrolyte Sustains High-Voltage Lithium Metal Batteries. *Angew. Chem., Int. Ed.* **2018**, *57* (43), 14055–14059.

(6) Amanollahi, H.; Moussavi, G.; Giannakis, S. VUV/Fe(II)/H₂O₂ as a novel integrated process for advanced oxidation of methyl tert-butyl ether (MTBE) in water at neutral pH: Process intensification and mechanistic aspects. *Water Res.* **2019**, *166*, 115061.

(7) Wang, D.; Yang, B.; Zhai, X.; Zhou, L. Synthesis of Diethyl Carbonate by Catalytic Alcoholysis of Urea. *Fuel Process. Technol.* **2007**, *88* (8), 807–812.

(8) Bruno, T. J.; Wolk, A.; Naydich, A.; Huber, M. L. Composition-explicit Distillation Curves for Mixtures of Diesel Fuel with Dimethyl Carbonate and Diethyl Carbonate. *Energy Fuels* **2009**, *23* (8), 3989–3997.

(9) Yan, T.; Bing, W.; Xu, M.; Li, Y.; Yang, Y.; Cui, G.; Yang, L.; Wei, M. Acid–base sites Synergistic Catalysis over Mg–Zr–Al Mixed Metal Oxide toward Synthesis of Diethyl Carbonate. *RSC Adv.* **2018**, *8* (9), 4695–4702.

(10) Wang, P.; Liu, S.; Zhou, F.; Yang, B.; Alshammari, A. S.; Deng, Y. Catalytic Alcoholysis of Urea to Diethyl Carbonate over Calcined Mg–Zn–Al Hydrotalcite. *RSC Adv.* **2015**, *5* (25), 19534–19540.

(11) Zhao, L.-C.; Hou, Z.-Q.; Liu, C.-Z.; Wang, Y.-Y.; Dai, L.-Y. A catalyst-free novel synthesis of diethyl carbonate from ethyl carbamate in supercritical ethanol. *Chin. Chem. Lett.* **2014**, *25* (10), 1395–1398.

(12) Keller, T.; Holtbruegge, J.; Niesbach, A.; Górkak, A. Transesterification of Dimethyl Carbonate with Ethanol To Form Ethyl Methyl Carbonate and Diethyl Carbonate: A Comprehensive Study on Chemical Equilibrium and Reaction Kinetics. *Ind. Eng. Chem. Res.* **2011**, *50* (19), 11073–11086.

(13) Murugan, C.; Bajaj, H. C. Synthesis of diethyl carbonate from dimethyl carbonate and ethanol using KF/Al₂O₃ as an efficient solid base catalyst. *Fuel Process. Technol.* **2011**, *92* (1), 77–82.

(14) Qiu, P.; Wang, L.; Jiang, X.; Yang, B. Synthesis of Diethyl Carbonate by the Combined Process of Transesterification with Distillation. *Energy Fuels* **2012**, *26* (2), 1254–1258.

(15) Zhang, Y.; Ji, Z.; Xu, R.; Fang, Y. Experimental and Kinetic Studies on a Homogeneous System for Diethyl Carbonate Synthesis by Transesterification. *Chem. Eng. Technol.* **2012**, *35* (4), 693–699.

(16) Leino, E.; Mäki-Arvela, P.; Eta, V.; Murzin, D. Y.; Salmi, T.; Mikkola, J. P. Conventional Synthesis Methods of Short-Chain DialkylCarbonates and Novel Production Technology via Direct route from Alcohol and waste CO₂. *Appl. Catal., A* **2010**, *383* (1), 1–13.

(17) Arbeláez, O.; Orrego, A.; Bustamante, F.; Villa, A. L. Direct Synthesis of Diethyl Carbonate from CO₂ and CH₃CH₂OH Over Cu–Ni/AC Catalyst. *Top. Catal.* **2012**, *55* (7–10), 668–672.

(18) Leino, E.; Kumar, N.; Mäki-Arvela, P.; Rautio, A.-R.; Dahl, J.; Roine, J.; Mikkola, J.-P. Synthesis and characterization of ceria-supported catalysts for carbon dioxide transformation to diethyl carbonate. *Catal. Today* **2018**, *306*, 128–137.

(19) Dunn, B. C.; Guenneau, C.; Hilton, S. A.; Pahnke, J.; Eyring, E. M.; Dworzanski, J.; Meuzelaar, H. L. C.; Hu, J. Z.; Solum, M. S.; Pugmire, R. J. Production of Diethyl Carbonate from Ethanol and Carbon Monoxide over a Heterogeneous Catalyst. *Energy Fuels* **2002**, *16* (1), 177–181.

(20) Shukla, K.; Srivastava, V. C. Diethyl Carbonate: Critical Review of Synthesis routes, Catalysts used and Engineering aspects. *RSC Adv.* **2016**, *6* (39), 32624–32645.

(21) Shukla, K.; Srivastava, V. C. Synthesis of organic carbonates from alcoholysis of urea: A review. *Catal. Rev.: Sci. Eng.* **2017**, *59* (1), 1–43.

(22) Shukla, K.; Srivastava, V. C. Synthesis of diethyl carbonate from ethanol through different routes: A thermodynamic and comparative analysis. *Can. J. Chem. Eng.* **2018**, *96* (1), 414–420.

(23) Xiong, H.; Mo, W.; Hu, J.; Bai, R.; Li, G. CuClPhen/NMI in Homogeneous Carbonylation for Synthesis of Diethyl Carbonate: Highly Active Catalyst and Corrosion Inhibitor. *Ind. Eng. Chem. Res.* **2009**, *48* (24), 10845–10849.

(24) Wang, H.; Zhang, H.; Hu, J.; Wang, G.; Deng, Z. Metal-Halide/Ionic-Liquid Oxidative Carbonylation of Ethanol to Synthesize

- Diethyl Carbonate with High Activity and Low Corrosion. *Chemistry Select* **2019**, *4* (45), 13265–13270.
- (25) Zhang, P.; Zhang, Z.; Wang, S.; Ma, X. A new type of catalyst PdCl₂/Cu-HMS for synthesis of diethyl carbonate by oxidative carbonylation of ethanol. *Catal. Commun.* **2007**, *8* (1), 21–26.
- (26) Briggs, D. N.; Lawrence, K. H.; Bell, A. T. An investigation of carbon-supported CuCl₂/PdCl₂ catalysts for diethyl carbonate synthesis. *Appl. Catal., A* **2009**, *366* (1), 71–83.
- (27) Zhang, P.; Ma, X. Catalytic synthesis of diethyl carbonate by oxidative carbonylation of ethanol over PdCl₂/Cu-HMS catalyst. *Chem. Eng. J.* **2010**, *163* (1), 93–97.
- (28) Shen, Y.; Wang, S.; Huang, S.; Li, Z.; Ma, X. DFT investigations of the reaction mechanism of diethyl carbonate synthesis catalyzed by Cu(I)/β or Pd(II)/β zeolites. *Appl. Surf. Sci.* **2014**, *308*, 237–246.
- (29) Ren, J.; Yang, J.; Wang, W.; Guo, H.; Zuo, Z.; Lin, J.; Li, Z. A DFT study of DMC formation on Rh-doped Cu/AC surfaces. *Int. J. Quantum Chem.* **2015**, *115* (13), 853–858.
- (30) Huang, S.; Zhang, J.; Wang, Y.; Chen, P.; Wang, S.; Ma, X. Insight into the Tunable CuY Catalyst for Diethyl Carbonate by Oxy carbonylation: Preparation Methods and Precursors. *Ind. Eng. Chem. Res.* **2014**, *53* (14), 5838–5845.
- (31) Fan, R.; Chen, C.; Han, M.; Gong, W.; Zhang, H.; Zhang, Y.; Zhao, H.; Wang, G. Highly Dispersed Copper Nanoparticles Supported on Activated Carbon as an Efficient Catalyst for Selective Reduction of Vanillin. *Small* **2018**, *14* (36), 1801953.
- (32) Wang, D.; Yang, G.; Ma, Q.; Wu, M.; Tan, Y.; Yoneyama, Y.; Tsubaki, N. Confinement Effect of Carbon Nanotubes: Copper Nanoparticles Filled Carbon Nanotubes for Hydrogenation of Methyl Acetate. *ACS Catal.* **2012**, *2* (9), 1958–1966.
- (33) Kang, M.; Bae, Y.-S.; Lee, C.-H. Effect of heat treatment of activated carbon supports on the loading and activity of Pt catalyst. *Carbon* **2005**, *43* (7), 1512–1516.
- (34) Yang, Y.; Jia, L.; Hou, B.; Li, D.; Wang, J.; Sun, Y. The oxidizing pretreatment-mediated auto reduction behaviour of cobalt nanoparticles supported on ordered mesoporous carbon for Fischer-Tropsch synthesis. *Catal. Sci. Technol.* **2014**, *4* (3), 717–728.
- (35) Amano, F.; Tanaka, T.; Funabiki, T. Auto-reduction of Cu(II) species supported on Al₂O₃ to Cu(I) by thermovacuum treatment. *J. Mol. Catal. A: Chem.* **2004**, *221* (1), 89–95.
- (36) Yin, H.; Cui, Z.; Wang, L.; Nie, Q. In situ reduction of the Cu/Cu₂O/carbon spheres composite for enzymaticless glucose sensors. *Sens. Actuators, B* **2016**, *222*, 1018–1023.
- (37) Chen, B.; Li, F.; Huang, Z.; Yuan, G. Carbon-coated Cu-Co bimetallic nanoparticles as selective and recyclable catalysts for production of biofuel 2,5-dimethylfuran. *Appl. Catal., B* **2017**, *200*, 192–199.
- (38) Chen, L.-F.; Guo, P.-J.; Qiao, M.-H.; Yan, S.-R.; Li, H.-X.; Shen, W.; Xu, H.-L.; Fan, K.-N. Cu/SiO₂ catalysts prepared by the ammonia-evaporation method: Texture, structure, and catalytic performance in hydrogenation of dimethyl oxalate to ethylene glycol. *J. Catal.* **2008**, *257* (1), 172–180.
- (39) Priyanka; Subbaramaiah, V.; Srivastava, V. C.; Mall, I. D. Catalytic oxidation of nitrobenzene by copper loaded activated carbon. *Sep. Purif. Technol.* **2014**, *125*, 284–290.
- (40) Siegfried, M. J.; Choi, K. S. Electrochemical Crystallization of Cuprous Oxide with Systematic Shape Evolution. *Adv. Mater.* **2004**, *16* (19), 1743–1746.
- (41) Gordon, A. S.; Knipe, R. H. The Explosive Reaction of Carbon Monoxide and Oxygen at the Second Explosion Limit in Quartz Vessels. *J. Phys. Chem.* **1955**, *59* (11), 1160–1165.
- (42) Paletti, G.; Peddinti, N.; Gajula, N.; Kadharabechi, V.; Rao, K. S. R.; Burri, D. R. Direct ethanol condensation to diethyl acetal in the vapour phase at atmospheric pressure over CuNP/SBA-15 catalysts. *New J. Chem.* **2019**, *43* (25), 10003–10011.
- (43) Zheng, X.; Bell, A. T. A Theoretical Investigation of Dimethyl Carbonate Synthesis on Cu-Y Zeolite. *J. Phys. Chem. C* **2008**, *112* (13), 5043–5047.
- (44) Zhang, Y.; Bell, A. T. The mechanism of dimethyl carbonate synthesis on Cu-exchanged zeolite Y. *J. Catal.* **2008**, *255* (2), 153–161.
- (45) Zhang, R.; Song, L.; Wang, B.; Li, Z. A density functional theory investigation on the mechanism and kinetics of dimethyl carbonate formation on Cu₂O catalyst. *J. Comput. Chem.* **2012**, *33* (11), 1101–1110.
- (46) Ren, J.; Wang, W.; Wang, D.; Zuo, Z.; Lin, J.; Li, Z. A theoretical investigation on the mechanism of dimethyl carbonate formation on Cu/AC catalyst. *Appl. Catal., A* **2014**, *472*, 47–52.
- (47) Ren, J.; Hao, P.; Sun, W.; Shi, R.; Liu, S. Ordered mesoporous silica-carbon-supported copper catalyst as an efficient and stable catalyst for catalytic oxidative carbonylation. *Chem. Eng. J.* **2017**, *328*, 673–682.
- (48) Briggs, D. N.; Bong, G.; Leong, E.; Oei, K.; Lestari, G.; Bell, A. T. Effects of support composition and pretreatment on the activity and selectivity of carbon-supported PdCu_nCl_x catalysts for the synthesis of diethyl carbonate. *J. Catal.* **2010**, *276* (2), 215–228.
- (49) Anderson, S. A.; Root, T. W. Investigation of the effect of carbon monoxide on the oxidative carbonylation of methanol to dimethyl carbonate over Cu+X and Cu+ZSM-5 zeolites. *J. Mol. Catal. A: Chem.* **2004**, *220* (2), 247–255.
- (50) Anderson, S. A.; Root, T. W. Kinetic studies of carbonylation of methanol to dimethyl carbonate over Cu+X zeolite catalyst. *J. Catal.* **2003**, *217* (2), 396–405.
- (51) Gajdos, M.; Hafner, J. CO adsorption on Cu(111) and Cu(001) surfaces: improving site preference in DFT calculations. *Surf. Sci.* **2005**, *590*, 117–126.
- (52) Zuo, Z.; Huang, W.; Han, P.; Li, Z. Solvent effects for CO and H₂ adsorption on Cu₂O (111) surface: A density functional theory study. *Appl. Surf. Sci.* **2010**, *256* (8), 2357–2362.